Structural Evolution of Water-in-Propylene Carbonate Mixtures Revealed by Experimental Raman Spectroscopy and Molecular Dynamics

Jessica B. Clark[†], Tai Bowling-Charles[†], Shamma Jabeen Proma[†], Biswajit Biswas[†], David T. Limmer[‡], Heather C. Allen[†*]

†Department of Chemistry & Biochemistry, The Ohio State University, Columbus, Ohio 43210, USA

‡Department of Chemistry, University of California, Berkeley, California 94720, USA

Materials Sciences Division, Lawrence Berkeley National Laboratory, Berkeley, California 94720, USA

Chemical Sciences Division, Lawrence Berkeley National Laboratory, Berkeley, California 94720, USA

Kavli Energy NanoScience Institute, Berkeley, California 94720, USA

Corresponding author

* Heather C. Allen, allen@chemistry.ohio-state.edu

Abstract

The liquid structure of systems wherein water is limited in concentration or through geometry is of great interest in various fields such as biology, materials science, and electrochemistry. Here, we present a combined polarized Raman and molecular dynamics investigation of the structural changes that occur as water is added incrementally to propylene carbonate (PC), a polar, aprotic solvent that is important in lithium-ion batteries. Polarized Raman spectra of PC solutions were collected for water mole fractions $0.003 \leq \chi_{water} \leq 0.296$, which encompasses the solubility range of water in PC. Analysis of the polarized carbonyl Raman band in conjunction with simulations demonstrated that the bulk structure of the solvent remained unperturbed upon the addition of water. Experimental spectra in the O-H stretching region were decomposed through Gaussian fitting into sub-bands and studies on dilute HOD in H_2O. With the aid of simulations, we identified these different bands as water arrangements having different degrees of hydrogen bonding. The observed water structure within PC indicates that water tends to self-aggregate, forming a hydrogen bond network that is distinctly

different from the bulk and dependent on concentration. For example, at moderate concentrations, the most likely aggregate structures are chains of water molecules, each with two hydrogen bonds on average.

Introduction

The structure and properties of water within complex environments is of fundamental interest due to its potential to reveal new insights into the dynamic hydrogen bonding network of water and its many anomalous bulk properties which have confounded the community for decades.[1,2] When water is limited in quantity and geometric configuration by physical or chemical constraints, its properties often differ significantly from those of a bulk liquid.[3–5] It is necessary to understand how the properties of water are altered in these environments in order to establish the limits at which bulk properties begin to arise or break down. This knowledge aids in the understanding of the fundamental microscopic mechanisms that govern water's macroscopic properties.

There has been significant study of the structure of water in systems with well-defined boundaries such as in confinement within reverse micelles[3,6] carbon nanotubes,[7,8] metal-organic frameworks,[9,10] and silica pores[11]. However, the study of water in disordered, dynamic environments such as binary mixtures has been more limited.[12–17] Notable exceptions are water in ionic liquids, which have gained significant interest in recent years.[16–19] Studies of ionic liquid binary mixtures with water reveal nanoscopic aggregation of water within the solvent (i.e. formation of a nanoconfined "water pocket") that is strongly dependent on the chemical structure of the ionic liquid.[16–18,20] Using small angle x-ray and neutron scattering, Abe and coworkers found that the "water pocket" formed in the ionic liquid [C_4mim][NO_3] has slow orientational dynamics and weak hydrogen bonds due to the nanoconfined nature of the system.[17]

In contrast to studies of water in ionic liquids, studies investigating binary mixtures of dilute water dispersed in dipolar, aprotic, organic solvents are more limited.[12,14,21–25] Studies in the late 1960s

showed that within partially chlorinated hydrocarbon solvents, water formed small clusters with itself (dimers to tetramers), but there was disagreement concerning the primary species.[25] In comparison to the previous study, Shultz and coworkers revealed that water exists as monomers in the non-polar solvent CCl_4 and that that the rotational motion of the monomers is greatly restricted by the solvating environment.[26] In hydrogen bond accepting solvents such as amines and ketones, water self-association has been observed and formation of the trimer species has been proposed.[12,24] In such systems, water exists under dynamic confinement by the polar, aprotic solvents due to a balance of intermolecular interactions. The structural characterization of these binary mixtures provides information that is critical in multiple materials applications such as ion solvation in electrolyte solutions.[27–29]

Propylene carbonate (PC) is a commonly used solvent in lithium-ion batteries, where it is typically mixed with linear carbonates to provide optimal charge stabilization and transport.[29–37] One of the pitfalls of these electrolyte solutions is the hygroscopicity of PC, which can result in water contamination. This contamination causes hydrolysis of $LiPF_6$ to HF and significantly impedes battery performance.[38,39] It is therefore critical to understand the solvation structure of water in PC.[32,36–39] PC has unique chemical and physical properties that make it a well-suited solvent for studies of water structure under dynamic confinement. PC has a high dielectric constant (64.40 at 25 °C) and dipole moment (4.94 D).[40] Unlike many other similar organic solvents, it cannot act as a hydrogen bond donor, only as an acceptor. As a result, some of the chemical complexity that exists in hydrogen bond donating solvents is removed, enabling simpler structural characterization.

The behavior of water in a binary solution with PC has been evaluated in two notable previous studies, yet there is disagreement between the proposed water structure. The first study by Grunwald and coworkers evaluated mixtures of PC and water in the concentration range 0-3.5 m ($\chi_{water} \leq 0.26$) using FTIR and ^{1}H NMR spectroscopies.[12] From this study, it was concluded that water primarily

forms monomers and dimers when solvated in PC and that cyclic trimers or other highly coordinated species do not form. Then in a second study, Dei and coworkers used surface tensiometry, differential scanning calorimetry, and FTIR spectroscopy to investigate mixtures of PC and water in the molar ratio range of $0.041 \leq \chi_{water} \leq 0.33$.[14] In contrast to the former study, the authors claim that monomers and dimers are the primary species only under very limited water conditions ($\chi_{water} < 0.14$). Once the water concentration exceeds the threshold, the authors observe that water shifts from being fully solvated by PC to forming stronger solute-solute interactions in trimers structures, a finding that is inconsistent with the older work by Grunwald et al. One aim of the present work is to shed new light on water structure within PC using polarized Raman spectroscopy and highly advanced, modern computational methods.

In the analysis of water's structure, vibrational spectroscopy is often employed due to its high sensitivity to the local environment of the molecule(s) being studied.[41–43] Raman spectroscopy in particular gives information relating to changes in intra- and intermolecular interactions making it well-suited for evaluating the changing interactions between water and PC.[41] In its liquid state, water forms four hydrogen bonds in an approximately tetrahedral geometry, on average. These hydrogen bonds are highly dynamic and fluctuate on a picosecond timescale causing a distribution of hydrogen bond configurations with varying bond strengths.[44,45] This phenomenon results in a broad band in the vibrational spectrum that corresponds to the distribution of O-H oscillator strengths.[41] Using a multi-state model, these hydrogen bond configurations have been shown to be spectrally distinguishable and can be resolved by fitting the spectral region to a number of Gaussian profiles which characterize the hydrogen bond structure.[6,42,43,46]

In this study, we evaluate the structure of dilute water in PC as the concentration is increased from $\chi_{water} = 0.003$ up to saturation ($\chi_{water} = 0.296$). Analysis of the O-H stretching and carbonyl regions of the Raman spectra reveals a hydrogen bond structure that is distinctly different from bulk water and

highly concentration dependent. The noncoincidence effect (NCE) in the polarized carbonyl Raman band provides insight into structural changes in PC due to water solvation. Isotopic dilution spectroscopic experiments (10% HOD in D_2O) bridge the gap between experiment and simulations as well as highlight the extent of intramolecular vibrational coupling within water aggregates. Molecular dynamics simulation results find that water associates with itself in PC more than previous experimental inferences[12,14] and suggests the most likely structure of the aggregates and their compositional evolution. Our analysis herein provides a resolution to water's unique structure within PC.

Methods

Materials and Sample Preparation

Solutions of dilute water dispersed in PC were prepared in the concentration range of $0.003 \leq \chi_{water} \leq 0.296$. These concentrations span the water-in-PC solubility range, stopping near the known miscibility gap ($0.33 \leq \chi_{water} \leq 0.95$ at 20 °C) of the two liquids.[14] PC/water solutions were prepared by the incremental addition of ultrapure water (Milli-Q Advantage A10, resistivity 18.2 MΩ) to 3.2626 ± 0.0017 g of PC (Sigma-Aldrich, ≥ 99.7%, anhydrous) in a standard quartz cuvette (Starna, 10 mm path length) that was sealed using a cap equipped with a silicone gasket to provide an air-tight seal. To limit water contamination of the solvent, a single-use sterile syringe and needle were used to transfer PC from the septum sealed bottle directly to the cuvette for immediate use without further purification. Thus, the purity of PC can be reasonably assumed to be that reported by the manufacturer (purity ≥ 99.65%, water content by Karl Fischer titration ≤ 0.002 %).[47] To further limit excess water in the system, the cuvette was dried in a 150 °C oven for at least 12 hours before use.

Prior to the addition of water, the Raman spectrum of the pure PC sample was acquired. To achieve the desired molar ratio, water was then added to the PC sample incrementally until phase

separation was reached. Phase separation occurred between a total of 240 and 260 μL of water added for all samples which corresponds to a water concentration in PC between χ_{water} = 0.29 and 0.31. The exact amount of water added to PC was determined by weighing the cuvette after each water addition (Mettler Toledo, XS104, ± 0.1 mg). Following each addition of water to PC, the sealed cuvette was manually shaken for at least 2 minutes then allowed to settle, undisturbed for 2 minutes prior to acquiring the polarized Raman spectra. Experiments were performed in duplicate at a room temperature of 20 °C.

Raman Spectroscopy

The custom-built Raman spectrometer used in the current work has been described previously.[48] Briefly, the Raman spectrometer consists of a diode-pumped continuous wave excitation laser (532 nm, 100:1 vertically (V) polarized, CrystaLaser) directly coupled to a Raman probe optical system (InPhotonics). Scattered light is collected using two independent fiber-optic cables which simultaneously collect the parallel (VV) and perpendicular (VH) polarized responses. The fiber optics are coupled to a spectrograph (IsoPlane 320, Princeton Instruments) using a 150 μm slit width and 600 g/mm grating (750 nm blaze). The two polarized signals are detected on separate regions of a LN_2-cooled CCD detector (Pylon 400BRX back-illuminated, Princeton Instruments). Spectra are collected by averaging 150 spectra using a 0.045 s exposure time. Laser power stability was ensured by taking the Raman spectrum of pure water following every 5 sample spectra. Intensity variations in the OH stretching region of the water spectrum were < 0.6% for all experiments.

Computational Studies

In order to validate the molecular inferences concerning the structure of water/PC mixtures, we developed a molecular dynamics simulation model. Using a GROMOS forcefield with an SPC/E water model, we simulated water/PC mixtures across a range of compositions between dilute solutions

and across the experimental miscibility gap.[49,50] All simulations were done under fixed number of molecules, temperature, and pressure using a Nose-Hoover thermostat and barostat.[51,52] The temperature and pressure were fixed to 298 K and 1 bar, respectfully. The number of molecules was equal to 200 PC molecules plus the number of water molecules necessary to fix the mole fraction between 0.04 and 0.22. Standard periodic boundary conditions, Ewald summation treatment of electrostatic interactions and a 2 fs timestep was employed in all simulations with the covalent hydrogen bonds held rigid with RATTLE.[53] Each composition was simulated for 10 ns, with an initial 1 ns simulation at elevated temperature of 400 K and fixed volume to equilibrate the initial composition fluctuations.

Results and Discussion

It is well known that the liquid structure of water is highly sensitive to its environment, yet there is still much debate over the microscopic mechanisms that govern water structure, particularly within systems where water is the solute. The aim of this study was to utilize a combined computational and experimental Raman approach to determine how dilute water partitions and interacts within a propylene carbonate (PC) solvent environment as water is increased up to the saturation limit. Structural changes within PC induced by the addition of water were also evaluated.

Raman Spectroscopy

The polarized Raman spectra of PC solutions were acquired as the water concentration was increased from a mole ratio of $\chi_{water} = 0.003$ to the saturation point (phase-separation) at $\chi_{water} = 0.296$. Particular attention is paid to the O-H stretching (3000 – 3800 cm^{-1}) and carbonyl regions (1700 – 1850 cm^{-1}) to determine water structure. The O-H stretching region consists of a broad band resulting from the population distribution of water hydrogen bond states, which are expected to evolve as more water is added to the system.[6,11,41,42] Deconvolution of the O-H stretching band into Gaussian sub-bands allowed for the characterization of water structure. The carbonyl band revealed interactions of

water with the solvating environment and developed a complete picture of how the PC bulk structure evolves to accommodate the solvation of water molecules.

Water Structure

The O-H stretching region of the PC/water Raman spectra after removing spectral contributions of pure PC through pre-processing is depicted in Figure 1. Further discussion of the spectral pre-processing procedure is presented in the Supplemental Information available below (S.I., see also Figures S1 & S2). These results demonstrate that the O-H stretching band increases in intensity and broadness as the water concentration is increased. It is difficult to determine the solvation structure of water from these spectra without further deconvolution of the hydrogen bonded sub-structure, therefore a Gaussian fitting was applied to this region. The fitting procedure is described in the S.I. and the converged parameters are included in Table S1 and Figure S3.

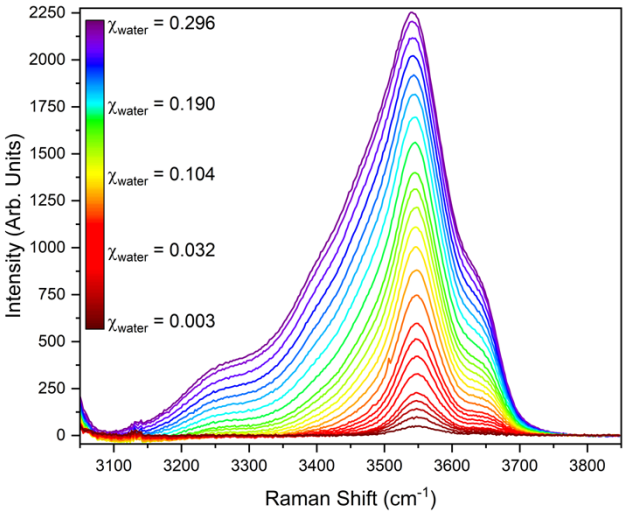

Figure 1. Raman spectra (VV polarization, O-H stretching region) of PC as water concentration is increased from 0.003 mole fraction (red) to 0.296 mole fraction (violet).

The number of Gaussian bands required for the fit was dependent on water concentration. In the low water concentration spectra ($\chi_{water} < 0.091$), only three Gaussian bands are required for the fit. A representative spectrum for the low water concentrations ($\chi_{water} = 0.013$) is plotted in Figure 2a. The highest frequency Gaussian is centered at 3643 cm^{-1} and is assigned to O-H groups that are

pointed towards the solvating PC molecules and are not participating in a hydrogen bond. This population is known as the "dangling-OH" and has been observed at various interfaces and in the hydration shells of hydrophobic moieties.[54–60] The dangling-OH vibrational band arising from the hydration shells of dissolved nonpolar groups has been reported to occur at ~3660 cm^{-1}.[54,56] In our spectra, this band is shifted to lower energy due to the solvating dielectric environment.

The second and third Gaussians occur at ~3550 and 3480 cm^{-1}, respectively, and can be collectively described as "partially coordinated." This means that the water molecules that make up these groups form between one and three hydrogen bonds, but still do not form the fully coordinated, tetrahedral structure.[14,43] Previous studies demonstrate that the partially coordinated water population can be further separated based on the degree of hydrogen bonding.[46,54,61,62] For example, when studying thermally excited water clusters, Suhm and coworkers concluded that the peak occurring near 3550 cm^{-1} in the FTIR spectrum could be assigned to the trimer water species.[61] They also observed a peak at ~3430 cm^{-1}, which was assigned to the tetramer water species. Similar band positions were observed in a study of water confined in silica slit pores where the band near 3550 cm^{-1} was assigned to water molecules which donate and accept a single hydrogen bond.[62] The band near 3450 cm^{-1} was assigned to all hydrogen bond configurations in which water is forming 3 hydrogen bonds.[62] Based on these studies, it is clear that the band we observe at 3550 cm^{-1} results from water molecules with low coordination and the band we observe at 3480 cm^{-1} results from water that is more coordinated in comparison. Therefore, we refer to the 3550 and 3480 cm^{-1} band populations as "low coordination" and "moderate coordination" water, respectively.

Beginning at χ_{water} = 0.091 up to the saturation point, a fourth Gaussian is needed for the fit. The final and lowest frequency band is centered at ~3260 cm^{-1} and is assigned to water that forms four hydrogen bonds in a tetrahedral geometry. This band can be observed in Figure 2b, where a representative spectrum for the high water concentrations (χ_{water} = 0.232) is plotted. We refer to this

population as "full coordination" water. This peak assignment has been well-established in the literature for both bulk and confined water.[11,43] In water clusters, this peak is only observed for hexamers or larger cluster sizes.[61]

Comparison of the low (Figure 2a) and high (Figure 2b) water concentration deconvolutions reveals that the largest spectral changes due to increasing water concentration occur for the moderate and full coordination water species. The fully coordinated water peak, which is initially not present, is observed as water is added to the system. The moderate coordination water peak significantly increases in broadness and intensity, accounting for much of the changes observed in the entire O-H stretching region.

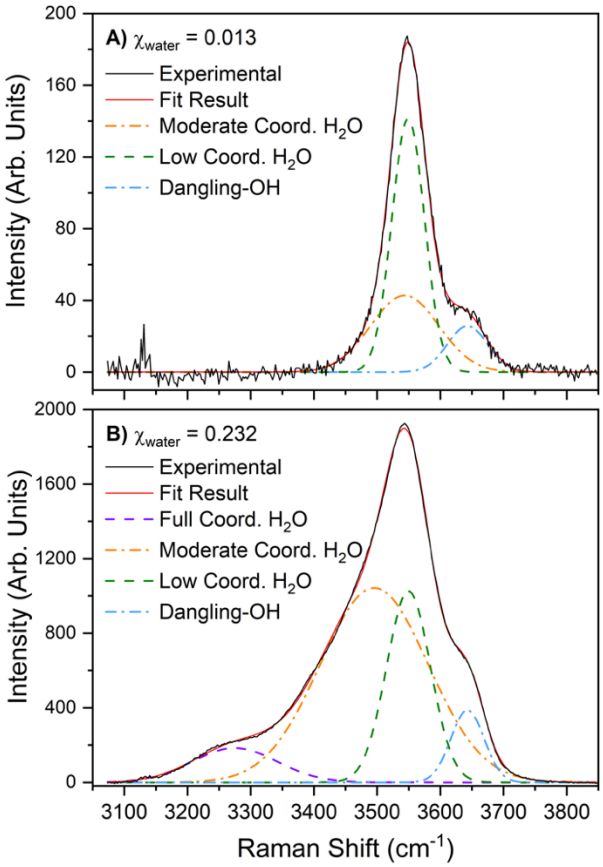

Figure 2. Gaussian deconvolution of experimental Raman O-H region for water concentrations χ_{water} = 0.013 (A) and 0.232 (B). Experimental (black) and fit (red) spectra are plotted with solid lines. Dashed lines represent Gaussian bands used to fit experimental spectra.

Analysis of the individual deconvoluted bands as a function of water concentration (Figure 3) allowed for further understanding of how the water structure in PC evolves. Upon the addition of water, the full coordination band (Figure 3a) increases in intensity and shifts significantly ($\Delta\nu = -70$ cm^{-1}) to lower frequencies (red-shifts). Similarly, the moderate coordination band (Figure 3b) increases in intensity and red-shifts ($\Delta\nu = -53$ cm^{-1}). The shifting of vibrational bands to lower frequency as a function of concentration is attributed to the strengthening of hydrogen bonds or other intermolecular interactions with the oscillator. Moreover, the O-H stretching region in Raman spectra has been shown to be sensitive to the degree of tetrahedral order within water, where the band shifts strongly to lower frequencies as the tetrahedral order is increased.[63] The observed red-shifts in the moderate and full coordination bands are consistent with the formation of ordered hydrogen bond configurations which have increasing tetrahedral character and stronger bonds.

The low coordination (Figure 3c) and dangling-OH (Figure 3d) bands behave similarly as the water concentration is increased. Both bands increase in intensity as a result of an increase in the total water molecules in the system. These Gaussian bands also do not undergo strong frequency shifts. The low coordination band increases in frequency (blue-shifts) by a total of 2 cm^{-1}. This can be attributed to intrinsic error in the fitting analysis or could be indicative of subtle weakening of the hydrogen bonds for this species. The frequency of the dangling-OH band did not change appreciably between the highest and lowest water concentration studied; therefore, it was held constant for all subsequent fittings (see S.I. below). The fact that the peak positions of the low coordination and dangling-OH bands do not change appreciably indicates that the water species that make up these populations do not undergo significant structural changes as the water concentration is increased.

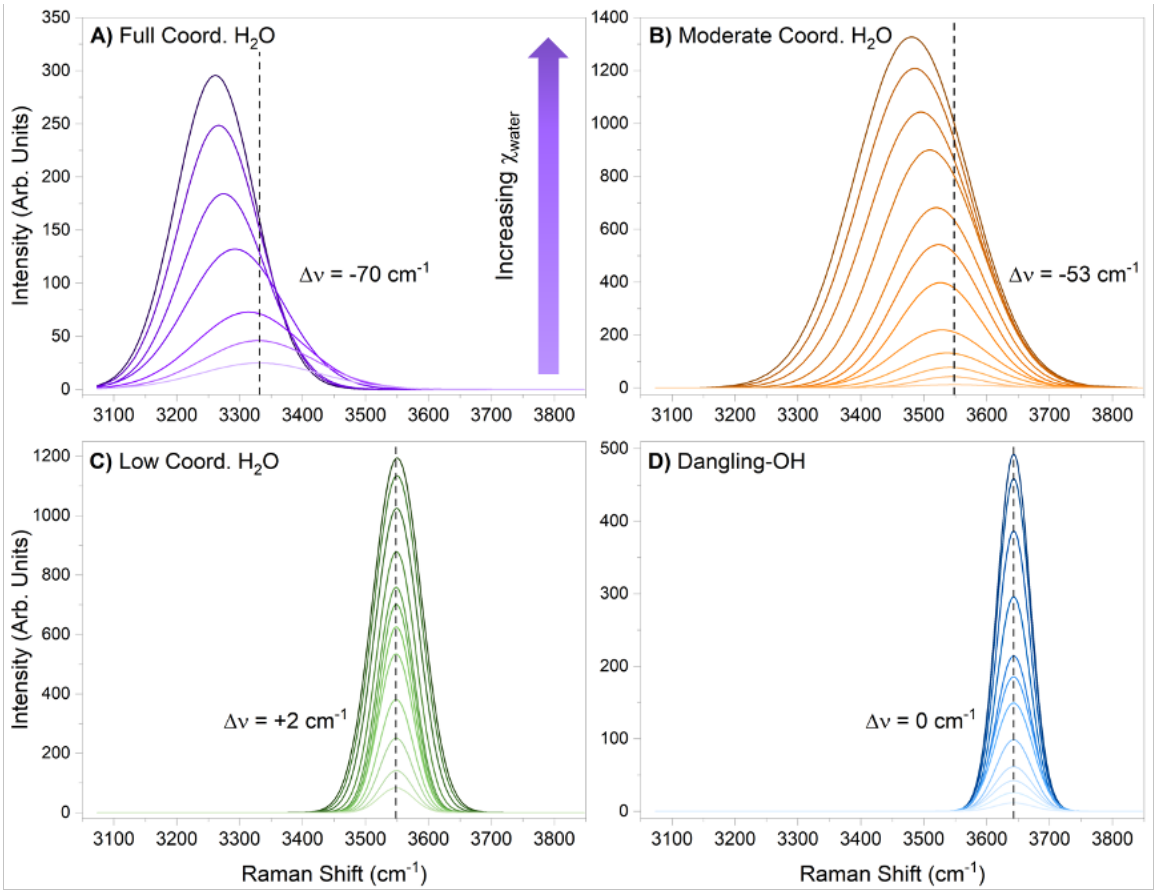

Figure 3. Evolution of the deconvoluted Gaussian bands as the water concentration in PC is increased. Each band corresponds to a different hydrogen bonded population of water; full coordination (A, violet), moderate coordination (B, orange), low coordination (C, green), and dangling-OH (D, blue). Darker colors correspond to higher water concentrations and dashed reference lines are set at peak position for lowest water concentration.

The present analysis of the Raman O-H stretching region assumes that water exists within one of four populations based on its hydrogen bonding state: dangling-OH, low coordination, moderate coordination, or full coordination. The O-H transition moment strength is assumed to remain constant across the individual solutions, therefore it follows that the total area of the O-H stretching band is the sum of the areas of the deconvoluted bands attributed to the different water population. Taking this into account, we calculated the percent of the total area taken up by the individual water populations as a function of water concentration. In Figure 4, the percent of the total O-H stretching area taken up by each Gaussian is plotted as a function of water mole fraction. This

plot demonstrates how the relative concentration of the water populations change as water is added to PC.

At the lowest water concentrations in PC, the low coordination population is present in the highest relative concentration. As water is added, the concentration of the low coordination state decreases sharply and levels off around χ_{water} = 0.20 with a total decrease of 41%. Correspondingly, the moderate coordination population sharply increases in relative concentration as water is added. The total increase in the contribution of this band is 34%. The inverse trend in the relative concentration of the low and moderate coordination states demonstrates a shift in hydrogen bond structure as water is added to PC. Under very dilute conditions, water molecules exist primarily in low coordination states and do not interact strongly with one another. As water concentration is increased, water structure shifts and a greater population of water exists in moderate and full coordination states. The leveling off of the relative concentration curves in Figure 4 indicates that this shift in structure is complete at χ_{water} = 0.20.

The full coordination and dangling-OH populations do not experience significant changes in relative concentration. The full coordination state is not present until χ_{water} = 0.091 is reached due to the low intensity of this band at more dilute concentrations. This band undergoes an overall relative concentration increase of 9%, which indicates that a larger fraction of the total water molecules exists in the most coordinated, tetrahedral state. This is only possible if water is interacting strongly with itself and forming aggregates larger than hexamers.[20] The relative concentration of the dangling-OH population remains approximately constant at 8%. This concentration of dangling-OH is higher than in bulk water where it is ~3%.[43] We conclude that the solvating PC environment yields a water hydrogen bonding structure that is disrupted from typical bulk water organization. Instead, PC supports a higher concentration of dangling-OH groups.

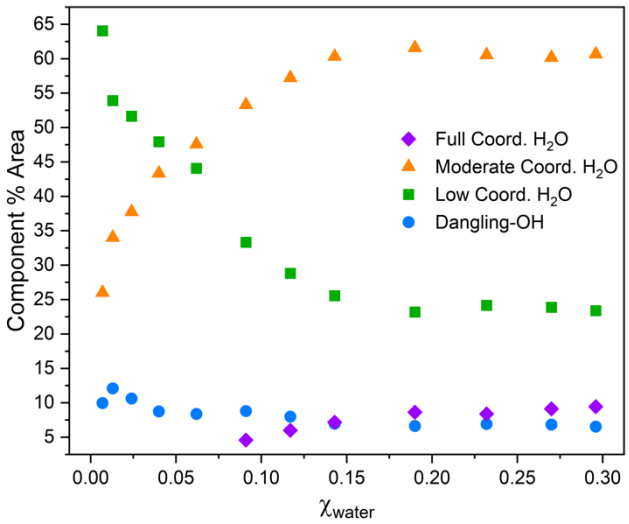

Figure 4. Percent of the total O-H stretching area taken up by each Gaussian band as a function of water concentration.

Based on the observed changes to the hydrogen-bonded sub-structure, we conclude that at low concentrations of water in PC, water does not self-associate to an appreciable extent. Instead, it is primarily solvated by weaker intermolecular interactions with PC. The presence of the 3480 and 3550 cm^{-1} bands at the lowest water concentration spectra suggest that a fraction of water molecules in PC form small aggregates such as dimers up to potentially tetramers and pentamers. We also conclude that concentrations above χ_{water} = 0.091, water self-associates to a greater extent, forming relatively large aggregates within the PC environment. The presence of the fully coordinated water peak indicates that a significant portion of clusters formed have increasing tetrahedral order and must be hexamers or larger. In contrast to previous conculsions,[12,14] we observe a gradual transition from mostly solvated water molecules to primarily aggregated water molecules in PC.

Using molecular dynamics (MD) simulations, we have quantified the degree of water clustering in PC by computing the average number of hydrogen bonds between water molecules as a function of bulk composition. Example snapshots from the MD simulations are shown in Figure 5a. These characteristic configurations show that water is well dispersed in the majority PC fluid. To accomplish this, we have employed a geometric criteria from Luzar and Chandler[64] for defining a hydrogen bond

(n_{HB}) as an oxygen-oxygen separation distance of less then 3.5 Å and an angle between the oxygen-oxygen displacement vector and the oxygen-hydrogen bond vector as less then 30°. The results of these calculations are shown in Figure 5b where we enumerate the probability $P(n_{HB})$ of both the number and type of hydrogen bond. Specifically, we have differentiated molecules that are double hydrogen bond donors (DD), double acceptors (AA), single acceptor-single donors (DA), or double-donor single acceptors (DDA). At χ_{water} = 0.04, water exists as a monomer 70% of the time, with the probability of dimers and trimers falling along Poisson statisics. At elevated water concentrations, the mostly likely structure becomes chains of water molecules each with two hydrogen bonds, one donated and the other accepting. The number of three and four coordinated water remains low, totalling only a combined 25% of solubilized water at the highest mole fractions considered, χ_{water} = 0.22. These basic trends agree qualitatively with those in Figure 4 from the Gaussian deconvolution of the experimental Raman spectra.

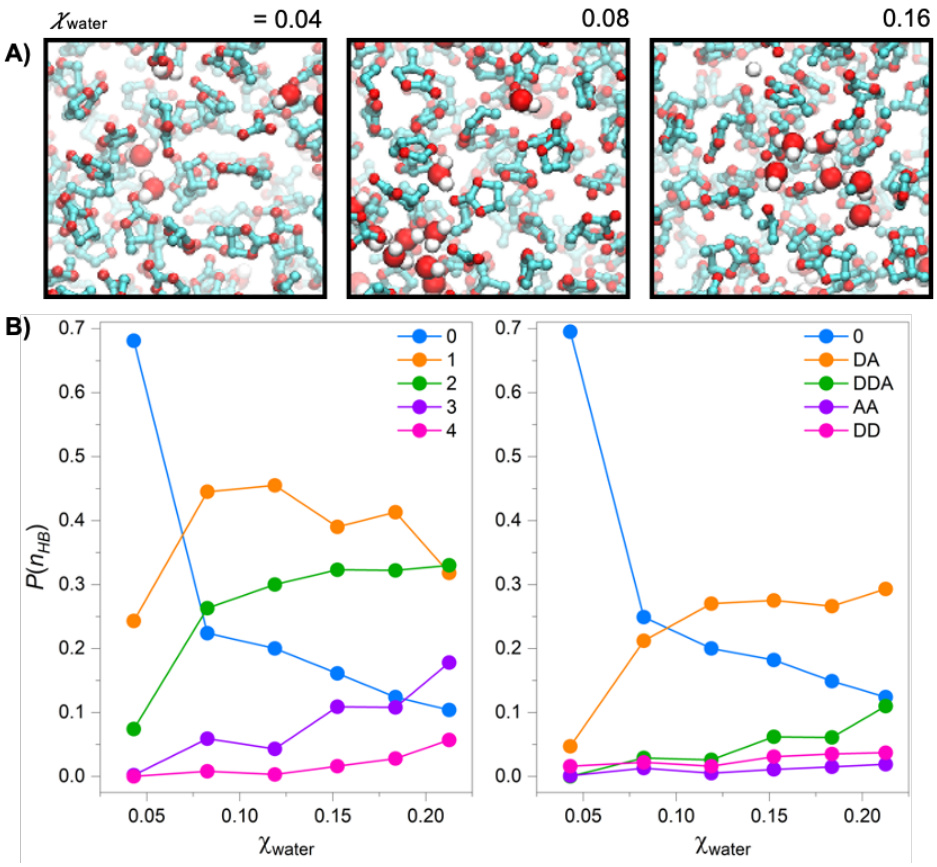

Figure 5. Molecular dynamic simulations of water-PC mixtures. A) Characteristic snapshots at different compositions. B) Probability of different hydrogen bond arrangements.

As inferred from the experimentally deconvolved Raman spectra, the simulations confirm that the O-H stretching frequency is determined by a large extent to the degree of hydrogen bonding between water molecules. To calculate the Raman spectra, we have employed a frequency map based approach.[65] Specifically, in the purely inhomogeneous broadening limit, the Raman lineshape is a probe of the local electric field, ξ along the OH bond vector.[66] This follows from the a Stark effect and first order perturbation theory between the oscillator and the surrounding bath such that the frequency shifts are given by $\omega - \omega_o = Q\xi$, where ω_o and Q are taken here as empirical parameters determined to best fit the lineshape. Specifically, a proceedure that has been employed by Geissler and coworkers in pure water and aqueous solutions, is to map the Raman lineshape to the distribution of electric fields acting on the hydrogen in the direction of the OH bond vector.[67] To validate this

approach, we have plotted in Figure 6a the distribution of electric fields on top of the experimentally measured OH stretching region of the Raman lineshape for diluted HOD in D_2O/PC mixtures. Using diluted HOD in D_2O, allows us to decouple the oscillators, and mitigate effects from delocalization of the vibrations.[68–71] As observed in past simulations,[72] this simple classical perspective on the Raman lineshape allows us to identify specific molecular structures that give rise to features in the relatively broad lineshape.

The simulation and experimental lineshape for dilute HOD match well over the compositions considered, with an asymmetric shape rising quickly at high fequencies and falling slowly at low frquencies. Notably sharp features in the H_2O in PC lineshape at 3250 cm^{-1} and 3650 cm^{-1} are less pronouced in the diluted HOD spectra and the corresponding simulations, suggesting that some of the structure results from delocalization of the oscillation. Upon increasing the concentration of water, the simulated spectra from the mapped frequencies in Figure 6b show the same basic trends as those observed experimentally, namely an increased broadening in the form of a lower frequency or, equivalently, a larger magnitude electric field. In the simulations, this growing mode at lower frequency is identified as the OH oscillator donating a hydrogen bond to another water molecule. No other motif strongly correlates with the increasing intensity, as only local hydrogen bonding produces such drammatically different local electric fields (see Figure S4).

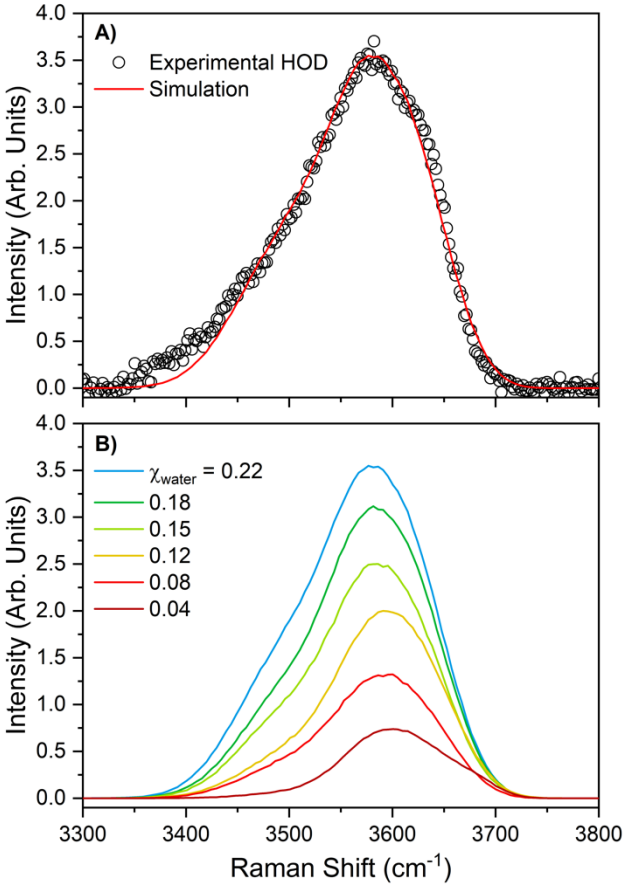

Figure 6. Raman spectra (OH stretching region) from molecular dynamics simulations of dilute HOD. A) Comparison of experimental spectra and frequency mapped spectra for 0.22 mole fraction. B) Simulated spectra as water concentration is increased from 0.04 mole fraction (red) to 0.22 mole fraction (blue).

Propylene Carbonate Structure

To gain insight into the effect that the addition of water has on the bulk structure of PC, the carbonyl region of the experimental and theoretical spectra were analyzed. The experimental carbonyl stretch Raman spectra as a function of water concentration are presented in Figure 7 with the theoretical spectra plotted in the inset. The carbonyl peak for pure PC has been reported to occur in the Raman spectrum at approx. 1780 cm^{-1}, with a Fermi resonance band causing a shoulder on the high-frequency side.[29,33,73] Here, we observe the carbonyl band for pure PC at 1779 cm^{-1}, where it undergoes a small red-shift ($\Delta\nu$ = ~2 cm^{-1}) and an overall decrease in intensity as the concentration

of water is increased (Figure 7). The decrease in intensity of the band is a result of the dilution of PC that occurs upon each addition of water. As described above, the red-shift that this band undergoes is indicative of strengthening intermolecular interactions with the oscillator. The carbonyl band in vibrational spectra has previously proven to be a sensitive probe for hydration structure, producing significant shifts (upwards of $\Delta\nu$ = 20-30 cm^{-1}) upon changes in hydration.[74–76] As a result, we assert that the water concentration-dependent red-shift of the carbonyl band is due to the formation of weak water-PC hydrogen bonding at this molecular site. These are in agreement with the molecular dynamic simulations, where the C=O stretch is computed in an analogous manner as those of the O-H stretch in water, using the electric field acting in the direction of the C=O bond vector.

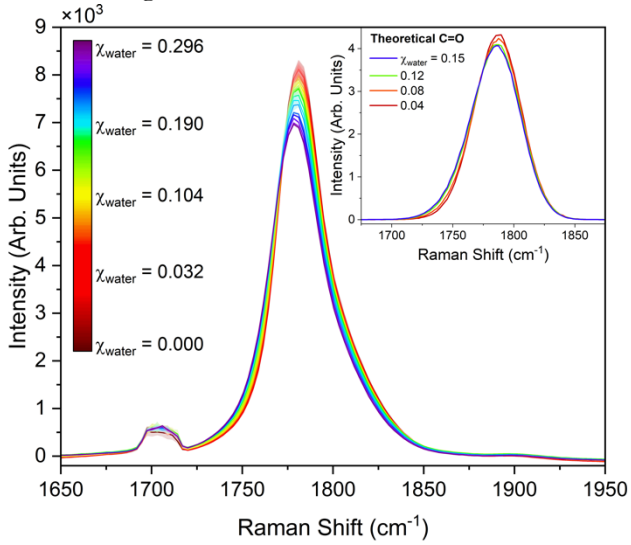

Figure 7. Raman spectra (VV polarization, carbonyl stretching region) of PC as water concentration is increased from χ_{water} = 0 (red) to 0.296 (violet). Band structure occurring at ~1710 cm^{-1} is a result of an artifact in the Raman optical system and does not correspond to molecular vibrations. Theoretical C=O stretching spectra are plotted in the inset.

Further information on structural changes in PC can be gained through consideration of the polarized Raman spectra in terms of the noncoincidence effect (NCE). The noncoincidence effect refers to the frequency difference between the isotropic and anisotropic components of a polarized Raman band ($\nu_{NCE} \equiv \nu_{isotropic} - \nu_{anisotropic}$), which originates from resonant vibrational energy transfer

between molecules that are intermolecularly coupled (e.g. by hydrogen bonds, permanent dipole moments, etc.).[77–80] Coupling between dipoles in pure propylene carbonate produces a relatively large and positive NCE in the carbonyl band, typically ~10 cm^{-1}.[29,80] In prior studies by the Allen lab and others, the NCE has been used to determine structural organization changes in dipolar liquids due to ion solvation.[29,48,77,78,81] For example, Giorgini and coworkers demonstrated that the addition of mono- and divalent cation salts to acetone produced large, negative carbonyl NCEs due to solvent clustering around the cation.[77,81]

In this study, we have calculated the isotropic (I_{iso}) and anisotropic (I_{ansio}) components of the carbonyl stretching band using the VV and VH polarized Raman spectra and the following equations: $I_{iso} = I_{VV} - \frac{4}{3} I_{VH}$ and $I_{aniso} = \frac{4}{3} I_{VH}$.[79] In Figure 8, the carbonyl band NCE resulting from pure PC (Figure 8a) and from the PC solution with the maximum water concentration, χ_{water} = 0.296, (Figure 8b) are compared. The addition of water to PC causes a total NCE decrease of 0.5 cm^{-1}, which is consistent with the formation of weak hydrogen bonds between the carbonyl of PC and water.[78] The observed change in NCE as water is added to PC is small in comparison to previously reported carbonyl NCE changes in propylene carbonate as well as in other similar solvents.[29,73,81] Thus, we conclude that the bulk structure of PC is not significantly perturbed by the addition of water up to the solubility limit.

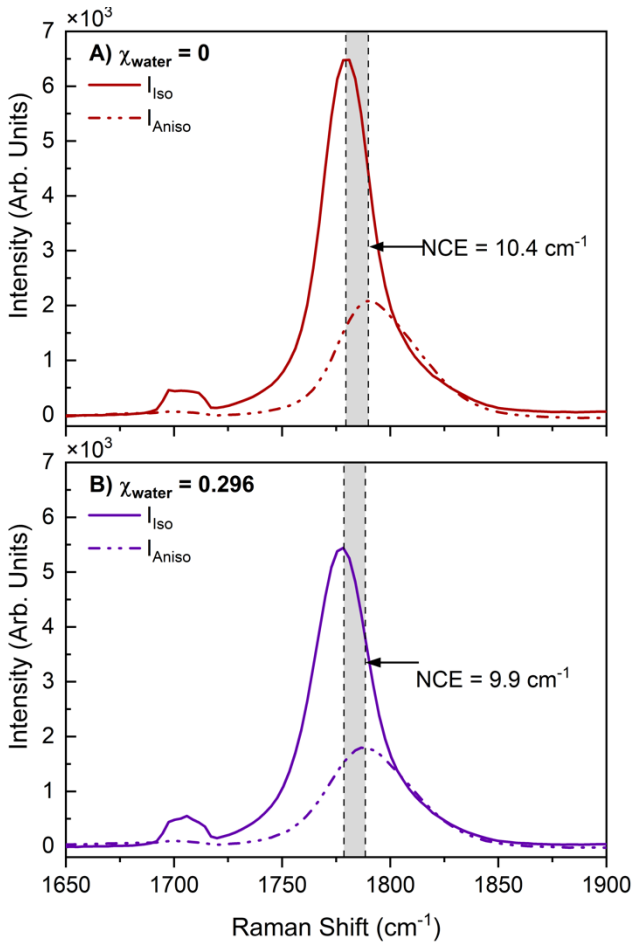

Figure 8. Isotropic (solid line) and anisotropic (dashed line) components of the polarized carbonyl Raman band for pure PC (A, red) and PC with water added to a mole fraction of 0.296 (B, violet). Dashed reference lines are included at the carbonyl peak position (determined by Gaussian fitting) for the isotropic and anisotropic components. The shaded gray area represents the noncoincidence effect (difference in isotropic and anisotropic peak positions) for each solution.

Conclusions

In this work, we characterize water concentration-dependent structural changes of a PC/water binary system using polarized Raman spectroscopy and molecular dynamics simulations. Gaussian deconvolution of the OH region in the experimental spectra reveals a water hydrogen-bond structure that consists of either three or four sub-bands that are assigned based on the degree of hydrogen bonding. For water concentrations in PC less than $\chi_{water} = 0.091$, dangling-OH, low coordination, and

moderate coordination states are observed. Above this concentration, a fourth sub-band is observed, which corresponds to fully coordinated, tetrahedral water. As evidenced by the evolution of the water hydrogen bond sub-bands, water is primarily solvated by PC under dilute conditions and does not tend to form aggregates. Increasing the water concentration leads to an increase in tetrahedral water structure and indicates that water exists primarily in aggregates at higher concentrations. MD simulation results support this conclusion as well as provide additional insight into the size and type of aggregates formed. Simulations of the system where χ_{water} = 0.04 reveal that water exists as monomers 70% of the time, with dimers and trimers accounting for the remaining conformations. Interestingly, the simulations find that the mostly likely water structure at elevated concentrations is chains of water molecules, each with two hydrogen bonds. Experimental and simulation results show that the hydrogen bond structure of water is distinctly different from the bulk at all concentrations, where the presence of three and four coordinate water is lower and dangling-OH is higher in comparison to bulk. The bulk structure of PC is not significantly perturbed by the addition of water as demonstrated by a change in carbonyl NCE of only 0.5 cm^{-1} from pure PC to the highest water concentration in PC. Overall, the addition of water to PC results in a relatively unperturbed PC structure, yet water structure evolves in a highly concentration-dependent manner. This yields a distribution of hydrogen bonded states including linear chains as well as structures with more tetrahedral local order.

Supporting Information

Contents: Raman spectra of the O-H stretching region prior to spectral pre-processing along with discussion of the pre-processing method, details of Gaussian fitting procedure for the O-H stretching region and a compilation of all converged fit parameters, explanation of the electric field fluctuation decomposition applied to calculated Raman spectra.

Acknowledgements

The authors acknowledge support from the National Science Foundation through grant No. CHE-2102313. J.B.C. would like to thank A. Enders for insightful comments on the manuscript. The authors declare no competing financial interest.

References

(1) Ball, P. Water — an Enduring Mystery. *Nature* **2008**, *452* (7185), 291–292. https://doi.org/10.1038/452291a.
(2) Nilsson, A.; Pettersson, L. G. M. The Structural Origin of Anomalous Properties of Liquid Water. *Nat. Commun.* **2015**, *6* (1), 8998. https://doi.org/10.1038/ncomms9998.
(3) Fayer, M. D.; Levinger, N. E. Analysis of Water in Confined Geometries and at Interfaces. *Annu. Rev. Anal. Chem.* **2010**, *3* (1), 89–107. https://doi.org/10.1146/annurev-anchem-070109-103410.
(4) Corti, H. R.; Appignanesi, G. A.; Barbosa, M. C.; Bordin, J. R.; Calero, C.; Camisasca, G.; Elola, M. D.; Franzese, G.; Gallo, P.; Hassanali, A.; Huang, K.; Laria, D.; Menéndez, C. A.; de Oca, J. M. M.; Longinotti, M. P.; Rodriguez, J.; Rovere, M.; Scherlis, D.; Szleifer, I. Structure and Dynamics of Nanoconfined Water and Aqueous Solutions. *Eur. Phys. J. E* **2021**, *44* (11), 136. https://doi.org/10.1140/epje/s10189-021-00136-4.
(5) Shultz, M. J.; Baldelli, S.; Schnitzer, C.; Simonelli, D. Water Confined at the Liquid-Air Interface. In *Water in Confining Geometries*; Buch, V., Devlin, J. P., Eds.; Springer Series in Cluster Physics; Springer: Berlin, Heidelberg, 2003; pp 249–273. https://doi.org/10.1007/978-3-662-05231-0_12.
(6) Plastinin, I. V.; Burikov, S. A.; Dolenko, T. A. Laser Diagnostics of Reverse Microemulsions: Influence of the Size and Shape of Reverse Micelles on the Raman Spectrum on the Example of Water/AOT/Cyclohexane System. *J. Mol. Liq.* **2021**, *325*, 115153. https://doi.org/10.1016/j.molliq.2020.115153.
(7) Agrawal, K. V.; Shimizu, S.; Drahushuk, L. W.; Kilcoyne, D.; Strano, M. S. Observation of Extreme Phase Transition Temperatures of Water Confined inside Isolated Carbon Nanotubes. *Nat. Nanotechnol.* **2017**, *12* (3), 267–273. https://doi.org/10.1038/nnano.2016.254.
(8) Ma, X.; Cambré, S.; Wenseleers, W.; Doorn, S. K.; Htoon, H. Quasiphase Transition in a Single File of Water Molecules Encapsulated in (6,5) Carbon Nanotubes Observed by Temperature-Dependent Photoluminescence Spectroscopy. *Phys. Rev. Lett.* **2017**, *118* (2), 027402. https://doi.org/10.1103/PhysRevLett.118.027402.
(9) Rieth, A. J.; Hunter, K. M.; Dincă, M.; Paesani, F. Hydrogen Bonding Structure of Confined Water Templated by a Metal-Organic Framework with Open Metal Sites. *Nat. Commun.* **2019**, *10* (1), 4771. https://doi.org/10.1038/s41467-019-12751-z.
(10) Hunter, K. M.; Wagner, J. C.; Kalaj, M.; Cohen, S. M.; Xiong, W.; Paesani, F. Simulation Meets Experiment: Unraveling the Properties of Water in Metal–Organic Frameworks through Vibrational Spectroscopy. *J. Phys. Chem. C* **2021**, *125* (22), 12451–12460. https://doi.org/10.1021/acs.jpcc.1c03145.
(11) Crupi, V.; Interdonato, S.; Longo, F.; Majolino, D.; Migliardo, P.; Venuti, V. A New Insight on the Hydrogen Bonding Structures of Nanoconfined Water: A Raman Study. *J. Raman Spectrosc.* **2008**, *39* (2), 244–249. https://doi.org/10.1002/jrs.1857.
(12) Cogley, D. R.; Falk, M.; Butler, J. N.; Grunwald, E. Solvation and Self-Association of Water in Propylene Carbonate. *J. Phys. Chem.* **1972**, *76* (6), 855–864. https://doi.org/10.1021/j100650a011.

(13) Scherer, J. R.; Go, M. K.; Kint, S. Raman Spectra and Structure of Water in Dimethyl Sulfoxide. *J. Phys. Chem.* **1973**, *77* (17), 2108–2117. https://doi.org/10.1021/j100636a016.
(14) Dei, L.; Grassi, S. Peculiar Properties of Water as Solute. *J. Phys. Chem. B* **2006**, *110* (24), 12191–12197. https://doi.org/10.1021/jp060633l.
(15) Silva, P. L.; Bastos, E. L.; El Seoud, O. A. Solvation in Binary Mixtures of Water and Polar Aprotic Solvents: Theoretical Calculations of the Concentrations of Solvent−Water Hydrogen-Bonded Species and Application to Thermosolvatochromism of Polarity Probes. *J. Phys. Chem. B* **2007**, *111* (22), 6173–6180. https://doi.org/10.1021/jp068596l.
(16) Abe, H.; Yoshiichi, Y.; Hirano, T.; Ohkubo, T.; Kishimura, H. Hydrogen Bonding of Nanoconfined Water in Ionic Liquids. *J. Mol. Liq.* **2022**, 120383. https://doi.org/10.1016/j.molliq.2022.120383.
(17) Abe, H.; Takekiyo, T.; Yoshimura, Y.; Shimizu, A. Static and Dynamic Properties of Nano-Confined Water in Room-Temperature Ionic Liquids. *J. Mol. Liq.* **2019**, *290*, 111216. https://doi.org/10.1016/j.molliq.2019.111216.
(18) Yoshimura, Y.; Mori, T.; Kaneko, K.; Nogami, K.; Takekiyo, T.; Masuda, Y.; Shimizu, A. Confirmation of Local Water Structure Confined in Ionic Liquids Using H/D Exchange. *J. Mol. Liq.* **2019**, *286*, 110874. https://doi.org/10.1016/j.molliq.2019.04.151.
(19) Zhang, Z.; Zhang, Y.; Du, B.; Peng, Z. Liquid-like Poly(Ionic Liquid) as Electrolyte for Thermally Stable Lithium-Ion Battery. *ACS Omega* **2018**, *3* (9), 10564–10571. https://doi.org/10.1021/acsomega.8b01539.
(20) Hayes, R.; Imberti, S.; Warr, G. G.; Atkin, R. How Water Dissolves in Protic Ionic Liquids. *Angew. Chem. Int. Ed.* **2012**, *51* (30), 7468–7471. https://doi.org/10.1002/anie.201201973.
(21) Dickens, B.; Dickens, S. H. Estimation of Concentration and Bonding Environment of Water Dissolved in Common Solvents Using Near Infrared Absorptivity. *J. Res. Natl. Inst. Stand. Technol.* **1999**, *104* (2), 173–183.
(22) Ivanov, E. V.; Lebedeva, E. Yu. Volumetric Properties of H2O and D2O Solutions in Propylene Carbonate at T=(278.15, 288.15, 298.15, 308.15, and 318.15) K under Atmospheric Pressure. *J. Mol. Liq.* **2011**, *159* (2), 124–131. https://doi.org/10.1016/j.molliq.2010.12.009.
(23) Bonner, O. D.; Choi, Y. S. Hydrogen Bonding of Water in Organic Solvents. II. Change of Water Structure with Composition. *J. Phys. Chem.* **1974**, *78* (17), 1727–1731. https://doi.org/10.1021/j100610a010.
(24) Johnson, J. R.; Christian, S. D.; Affsprung, H. E. The Molecular Complexity of Water in Organic Solvents. Part III. *J. Chem. Soc. Inorg. Phys. Theor.* **1967**, No. 0, 1924–1928. https://doi.org/10.1039/J19670001924.
(25) Christian, S. D.; Taha, A. A.; Gash, B. W. Molecular Complexes of Water in Organic Solvents and in the Vapour Phase. *Q. Rev. Chem. Soc.* **1970**, *24* (1), 20. https://doi.org/10.1039/qr9702400020.
(26) Kuo, M.; Kamelamela, N.; Shultz, M. J. Rotational Structure of Water in a Hydrophobic Environment: Carbon Tetrachloride. *J. Phys. Chem. A* **2008**, *112* (6), 1214–1218. https://doi.org/10.1021/jp7097284.
(27) Liang, C.; Kwak, K.; Cho, M. Revealing the Solvation Structure and Dynamics of Carbonate Electrolytes in Lithium-Ion Batteries by Two-Dimensional Infrared Spectrum Modeling. *J. Phys. Chem. Lett.* **2017**, *8* (23), 5779–5784. https://doi.org/10.1021/acs.jpclett.7b02623.
(28) Hayes, R.; Warr, G. G.; Atkin, R. Structure and Nanostructure in Ionic Liquids. *Chem. Rev.* **2015**, *115* (13), 6357–6426. https://doi.org/10.1021/cr500411q.
(29) Giorgini, M. G.; Futamatagawa, K.; Torii, H.; Musso, M.; Cerini, S. Solvation Structure around the Li+ Ion in Mixed Cyclic/Linear Carbonate Solutions Unveiled by the Raman

Noncoincidence Effect. *J. Phys. Chem. Lett.* **2015**, *6* (16), 3296–3302. https://doi.org/10.1021/acs.jpclett.5b01524.
(30) Naji, A.; Ghanbaja, J.; Willmann, P.; Billaud, D. New Halogenated Additives to Propylene Carbonate-Based Electrolytes for Lithium-Ion Batteries. *Electrochimica Acta* **2000**, *45* (12), 1893–1899. https://doi.org/10.1016/S0013-4686(99)00410-7.
(31) Tasaki, K.; Goldberg, A.; Winter, M. On the Difference in Cycling Behaviors of Lithium-Ion Battery Cell between the Ethylene Carbonate- and Propylene Carbonate-Based Electrolytes. *Electrochimica Acta* **2011**, *56* (28), 10424–10435. https://doi.org/10.1016/j.electacta.2011.05.112.
(32) Aurbach, D.; Zaban, A. Impedance Spectroscopy of Lithium Electrodes: Part 1. General Behavior in Propylene Carbonate Solutions and the Correlation to Surface Chemistry and Cycling Efficiency. *J. Electroanal. Chem.* **1993**, *348* (1), 155–179. https://doi.org/10.1016/0022-0728(93)80129-6.
(33) Battisti, D.; Nazri, G. A.; Klassen, B.; Aroca, R. Vibrational Studies of Lithium Perchlorate in Propylene Carbonate Solutions. *J. Phys. Chem.* **1993**, *97* (22), 5826–5830. https://doi.org/10.1021/j100124a007.
(34) Xuan, X.; Wang, J.; Tang, J.; Qu, G.; Lu, J. A Vibrational Spectroscopic Study of Ion Solvation in Lithium Perchlorate/Propylene Carbonate Electrolyte. *Phys. Chem. Liq.* **2001**, *39* (3), 327–342. https://doi.org/10.1080/00319100108031666.
(35) Brennan, M. D.; Breedon, M.; Best, A. S.; Morishita, T.; Spencer, M. J. S. Surface Reactions of Ethylene Carbonate and Propylene Carbonate on the Li(001) Surface. *Electrochimica Acta* **2017**, *243*, 320–330. https://doi.org/10.1016/j.electacta.2017.04.163.
(36) Fulfer, K. D.; Kuroda, D. G. Solvation Structure and Dynamics of the Lithium Ion in Organic Carbonate-Based Electrolytes: A Time-Dependent Infrared Spectroscopy Study. *J. Phys. Chem. C* **2016**, *120* (42), 24011–24022. https://doi.org/10.1021/acs.jpcc.6b08607.
(37) Fulfer, K. D.; Galle Kankanamge, S. R.; Chen, X.; Woodard, K. T.; Kuroda, D. G. Elucidating the Mechanism behind the Infrared Spectral Features and Dynamics Observed in the Carbonyl Stretch Region of Organic Carbonates Interacting with Lithium Ions. *J. Chem. Phys.* **2021**, *154* (23), 234504. https://doi.org/10.1063/5.0049742.
(38) Stich, M.; Göttlinger, M.; Kurniawan, M.; Schmidt, U.; Bund, A. Hydrolysis of LiPF6 in Carbonate-Based Electrolytes for Lithium-Ion Batteries and in Aqueous Media. *J. Phys. Chem. C* **2018**, *122* (16), 8836–8842. https://doi.org/10.1021/acs.jpcc.8b02080.
(39) Li, W.; Lucht, B. L. Inhibition of the Detrimental Effects of Water Impurities in Lithium-Ion Batteries. *Electrochem. Solid-State Lett.* **2007**, *10* (4), A115. https://doi.org/10.1149/1.2458913.
(40) Muhuri, P. K.; Ghosh, S. K.; Hazra, D. K. Solubilities of Some Alkali-Metal Salts, Tetraphenylarsonium Chloride, and Tetraphenylphosphonium Bromide in Propylene Carbonate at 25.Degree.C Using the Ion-Selective Electrode Technique. *J. Chem. Eng. Data* **1993**, *38* (2), 242–244. https://doi.org/10.1021/je00010a014.
(41) Carey, D. M.; Korenowski, G. M. Measurement of the Raman Spectrum of Liquid Water. *J. Chem. Phys.* **1998**, *108* (7), 2669–2675. https://doi.org/10.1063/1.475659.
(42) Wang, Z.; Pakoulev, A.; Pang, Y.; Dlott, D. D. Vibrational Substructure in the OH Stretching Band of Water. *Chem. Phys. Lett.* **2003**, *378* (3), 281–288. https://doi.org/10.1016/S0009-2614(03)01267-3.
(43) Sun, Q. The Raman OH Stretching Bands of Liquid Water. *Vib. Spectrosc.* **2009**, *51* (2), 213–217. https://doi.org/10.1016/j.vibspec.2009.05.002.
(44) Nicodemus, R. A.; Ramasesha, K.; Roberts, S. T.; Tokmakoff, A. Hydrogen Bond Rearrangements in Water Probed with Temperature-Dependent 2D IR. *J. Phys. Chem. Lett.* **2010**, *1* (7), 1068–1072. https://doi.org/10.1021/jz100138z.

(45) Burikov, S.; Dolenko, T.; Patsaeva, S.; Starokurov, Y.; Yuzhakov, V. Raman and IR Spectroscopy Research on Hydrogen Bonding in Water-Ethanol Systems. *Mol. Phys.* **2010**, *108* (18), 2427–2436. https://doi.org/10.1080/00268976.2010.516277.
(46) Sun, Q. Local Statistical Interpretation for Water Structure. *Chem. Phys. Lett.* **2013**, *568–569*, 90–94. https://doi.org/10.1016/j.cplett.2013.03.065.
(47) *Propylene carbonate anhydrous, 99.7 108-32-7*. https://www.sigmaaldrich.com/US/en/product/sial/310328?gclid=Cj0KCQiAyracBhDoARIsACGFcS7weCHAT5_OlIWtLy6JvNcz06-j4DeGkq5UR4t4DxbnhJnzKzSJ-YMaAmauEALw_wcB&gclsrc=aw.ds (accessed 2022-12-05).
(48) Baumler, S. M.; V, W. H. H.; Allen, H. C. Hydration of Ferric Chloride and Nitrate in Aqueous Solutions: Water-Mediated Ion Pairing Revealed by Raman Spectroscopy. *Phys. Chem. Chem. Phys.* **2019**, *21* (35), 19172–19180. https://doi.org/10.1039/C9CP01392J.
(49) Berendsen, H. J. C.; Grigera, J. R.; Straatsma, T. P. The Missing Term in Effective Pair Potentials. *J. Phys. Chem.* **1987**, *91* (24), 6269–6271. https://doi.org/10.1021/j100308a038.
(50) Schuler, L. D.; Daura, X.; van Gunsteren, W. F. An Improved GROMOS96 Force Field for Aliphatic Hydrocarbons in the Condensed Phase. *J. Comput. Chem.* **2001**, *22* (11), 1205–1218. https://doi.org/10.1002/jcc.1078.
(51) Parrinello, M.; Rahman, A. Polymorphic Transitions in Single Crystals: A New Molecular Dynamics Method. *J. Appl. Phys.* **1981**, *52* (12), 7182–7190. https://doi.org/10.1063/1.328693.
(52) Martyna, G. J.; Tobias, D. J.; Klein, M. L. Constant Pressure Molecular Dynamics Algorithms. *J. Chem. Phys.* **1994**, *101* (5), 4177–4189. https://doi.org/10.1063/1.467468.
(53) Andersen, H. C. Rattle: A "Velocity" Version of the Shake Algorithm for Molecular Dynamics Calculations. *J. Comput. Phys.* **1983**, *52* (1), 24–34. https://doi.org/10.1016/0021-9991(83)90014-1.
(54) Tomlinson-Phillips, J.; Davis, J.; Ben-Amotz, D.; Spångberg, D.; Pejov, L.; Hermansson, K. Structure and Dynamics of Water Dangling OH Bonds in Hydrophobic Hydration Shells. Comparison of Simulation and Experiment. *J. Phys. Chem. A* **2011**, *115* (23), 6177–6183. https://doi.org/10.1021/jp111346s.
(55) Stirnemann, G.; Rossky, P. J.; Hynes, J. T.; Laage, D. Water Reorientation, Hydrogen-Bond Dynamics and 2D-IR Spectroscopy next to an Extended Hydrophobic Surface. *Faraday Discuss.* **2010**, *146* (0), 263–281. https://doi.org/10.1039/B925673C.
(56) Perera, P. N.; Fega, K. R.; Lawrence, C.; Sundstrom, E. J.; Tomlinson-Phillips, J.; Ben-Amotz, D. Observation of Water Dangling OH Bonds around Dissolved Nonpolar Groups. *Proc. Natl. Acad. Sci.* **2009**, *106* (30), 12230–12234. https://doi.org/10.1073/pnas.0903675106.
(57) Ma, G.; Chen, X.; Allen, H. C. Dangling OD Confined in a Langmuir Monolayer. *J. Am. Chem. Soc.* **2007**, *129* (45), 14053–14057. https://doi.org/10.1021/ja075806e.
(58) Scatena, L. F.; Brown, M. G.; Richmond, G. L. Water at Hydrophobic Surfaces: Weak Hydrogen Bonding and Strong Orientation Effects. *Science* **2001**, *292* (5518), 908–912.
(59) Medders, G. R.; Paesani, F. Dissecting the Molecular Structure of the Air/Water Interface from Quantum Simulations of the Sum-Frequency Generation Spectrum. *J. Am. Chem. Soc.* **2016**, *138* (11), 3912–3919.
(60) Sun, S.; Tang, F.; Imoto, S.; Moberg, D. R.; Ohto, T.; Paesani, F.; Bonn, M.; Backus, E. H.; Nagata, Y. Orientational Distribution of Free OH Groups of Interfacial Water Is Exponential. *Phys. Rev. Lett.* **2018**, *121* (24), 246101.
(61) Zischang, J.; Suhm, M. A. The OH Stretching Spectrum of Warm Water Clusters. *J. Chem. Phys.* **2014**, *140* (6), 064312. https://doi.org/10.1063/1.4865130.

(62) Senanayake, H. S.; Greathouse, J. A.; Ilgen, A. G.; Thompson, W. H. Simulations of the IR and Raman Spectra of Water Confined in Amorphous Silica Slit Pores. *J. Chem. Phys.* **2021**, *154* (10), 104503. https://doi.org/10.1063/5.0040739.
(63) Morawietz, T.; Marsalek, O.; Pattenaude, S. R.; Streacker, L. M.; Ben-Amotz, D.; Markland, T. E. The Interplay of Structure and Dynamics in the Raman Spectrum of Liquid Water over the Full Frequency and Temperature Range. *J. Phys. Chem. Lett.* **2018**, *9* (4), 851–857. https://doi.org/10.1021/acs.jpclett.8b00133.
(64) Luzar, A.; Chandler, D. Effect of Environment on Hydrogen Bond Dynamics in Liquid Water. *Phys. Rev. Lett.* **1996**, *76* (6), 928–931. https://doi.org/10.1103/PhysRevLett.76.928.
(65) Auer, B.; Kumar, R.; Schmidt, J. R.; Skinner, J. L. Hydrogen Bonding and Raman, IR, and 2D-IR Spectroscopy of Dilute HOD in Liquid D2O. *Proc. Natl. Acad. Sci.* **2007**, *104* (36), 14215–14220. https://doi.org/10.1073/pnas.0701482104.
(66) Fecko, C. J.; Eaves, J. D.; Loparo, J. J.; Tokmakoff, A.; Geissler, P. L. Ultrafast Hydrogen-Bond Dynamics in the Infrared Spectroscopy of Water. *Science* **2003**, *301* (5640), 1698–1702. https://doi.org/10.1126/science.1087251.
(67) Geissler, P. L. Water Interfaces, Solvation, and Spectroscopy. *Annu. Rev. Phys. Chem.* **2013**, *64* (1), 317–337. https://doi.org/10.1146/annurev-physchem-040412-110153.
(68) Eaves, J. D.; Loparo, J. J.; Fecko, C. J.; Roberts, S. T.; Tokmakoff, A.; Geissler, P. L. Hydrogen Bonds in Liquid Water Are Broken Only Fleetingly. *Proc. Natl. Acad. Sci.* **2005**, *102* (37), 13019–13022. https://doi.org/10.1073/pnas.0505125102.
(69) Asbury, J. B.; Steinel, T.; Stromberg, C.; Corcelli, S. A.; Lawrence, C. P.; Skinner, J. L.; Fayer, M. D. Water Dynamics: Vibrational Echo Correlation Spectroscopy and Comparison to Molecular Dynamics Simulations. *J. Phys. Chem. A* **2004**, *108* (7), 1107–1119. https://doi.org/10.1021/jp036266k.
(70) Corcelli, S. A.; Lawrence, C. P.; Skinner, J. L. Combined Electronic Structure/Molecular Dynamics Approach for Ultrafast Infrared Spectroscopy of Dilute HOD in Liquid H2O and D2O. *J. Chem. Phys.* **2004**, *120* (17), 8107–8117. https://doi.org/10.1063/1.1683072.
(71) Corcelli, S. A.; Skinner, J. L. Infrared and Raman Line Shapes of Dilute HOD in Liquid H2O and D2O from 10 to 90 C. *J. Phys. Chem. A* **2005**, *109* (28), 6154–6165.
(72) Smith, J. D.; Saykally, R. J.; Geissler, P. L. The Effects of Dissolved Halide Anions on Hydrogen Bonding in Liquid Water. *J. Am. Chem. Soc.* **2007**, *129* (45), 13847–13856. https://doi.org/10.1021/ja071933z.
(73) Janz, G. J.; Ambrose, J.; Coutts, J. W.; Downey, J. R. Raman Spectrum of Propylene Carbonate. *Spectrochim. Acta Part Mol. Spectrosc.* **1979**, *35* (2), 175–179. https://doi.org/10.1016/0584-8539(79)80181-6.
(74) Carter-Fenk, K. A.; Dommer, A. C.; Fiamingo, M. E.; Kim, J.; Amaro, R. E.; Allen, H. C. Calcium Bridging Drives Polysaccharide Co-Adsorption to a Proxy Sea Surface Microlayer. *Phys. Chem. Chem. Phys.* **2021**, *23* (30), 16401–16416. https://doi.org/10.1039/D1CP01407B.
(75) Dreier, L. B.; Bonn, M.; Backus, E. H. G. Hydration and Orientation of Carbonyl Groups in Oppositely Charged Lipid Monolayers on Water. *J. Phys. Chem. B* **2019**, *123* (5), 1085–1089. https://doi.org/10.1021/acs.jpcb.8b12297.
(76) Edington, S. C.; Flanagan, J. C.; Baiz, C. R. An Empirical IR Frequency Map for Ester C═O Stretching Vibrations. *J. Phys. Chem. A* **2016**, *120* (22), 3888–3896. https://doi.org/10.1021/acs.jpca.6b02887.
(77) Giorgini, M. G.; Torii, H.; Musso, M.; Venditti, G. Influence of Ions on the Structural Organization of Dipolar Liquids Probed by the Noncoincidence Effect: Experimental and

Quantum Chemical Results. *J. Phys. Chem. B* **2008**, *112* (25), 7506–7514. https://doi.org/10.1021/jp800252n.
(78) Vazquez de Vasquez, M. G.; Wellen Rudd, B. A.; Baer, M. D.; Beasley, E. E.; Allen, H. C. Role of Hydration in Magnesium versus Calcium Ion Pairing with Carboxylate: Solution and the Aqueous Interface. *J. Phys. Chem. B* **2021**, *125* (40), 11308–11319. https://doi.org/10.1021/acs.jpcb.1c06108.
(79) Kecki, Z.; Sokołowska, A. Crossing of Anisotropic and Isotropic Raman Components in the Intermolecular Resonance Coupling of Vibrations. IV—Methanol Solutions in Acetone. *J. Raman Spectrosc.* **1996**, *27* (5), 429–432. https://doi.org/10.1002/(SICI)1097-4555(199605)27:5<429::AID-JRS981>3.0.CO;2-O.
(80) Brodin, A.; Jacobsson, P. Dipolar Interaction and Molecular Ordering in Liquid Propylene Carbonate: Anomalous Dielectric Susceptibility and Raman Non-Coincidence Effect. *J. Mol. Liq.* **2011**, *164* (1), 17–21. https://doi.org/10.1016/j.molliq.2011.08.001.
(81) Giorgini, M. G.; Torii, H.; Musso, M. The Influence of Alkaline Earth Ions on the Structural Organization of Acetone Probed by the Noncoincidence Effect of the ν(CO) Band: Experimental and Quantum Chemical Results. *Phys. Chem. Chem. Phys.* **2009**, *12* (1), 183–192. https://doi.org/10.1039/B912164A.

Supporting Information

Structural Evolution of Water-in-Propylene Carbonate Mixtures Revealed by Experimental Raman Spectroscopy and Molecular Dynamics

Jessica B. Clark[†], Tai Bowling-Charles[†], Shamma Jabeen Proma[†], Biswajit Biswas[†], David T. Limmer[‡], Heather C. Allen[†*]

†Department of Chemistry & Biochemistry, The Ohio State University, Columbus, Ohio 43210, United States

‡ Department of Chemistry, University of California, Berkeley, California 94720, USA

Materials Sciences Division, Lawrence Berkesley National Laboratory, Berkeley, California 94720, USA

Chemical Sciences Division, Lawrence Berkeley National Laboratory, Berkeley, California 94720, USA

Kavli Energy NanoScience Institute, Berkeley, California 94720, USA

Corresponding author

* Heather C. Allen, allen@chemistry.ohio-state.edu

Table of Contents

Spectral Preprocessing

To account for small baseline shifts that occurred between replicates, the Raman spectra were aligned to a common baseline by taking the average of the final 50 intensity values (3750 – 3850 cm^{-1}) in each spectrum where there are no spectral features. The average value was then subtracted from the intensity of the corresponding spectrum. Following this baseline alignment, the average of the replicates was acquired. The OH stretching region of the Raman spectra following the baseline adjustment and averaging of replicates is depicted in Figure S1.

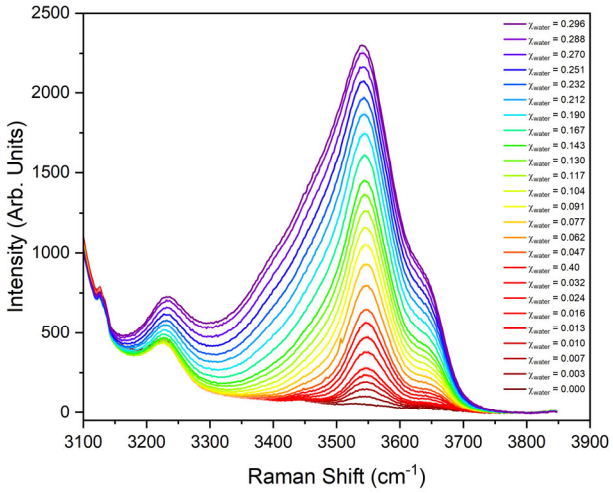

Figure S1. Raman spectra in the OH stretching region for propylene carbonate with increasing water concentrations (red $\chi_{water} = 0$ to violet $\chi_{water} = 0.296$). Spectra are plotted as the average of two replicates following baseline adjustment with the standard deviation plotted as shading.

Due to overlap with the intense C-H stretching modes that originate from PC, the OH stretching region has a steeply sloped baseline and is convoluted with the C-H stretching mode from PC at 3220 cm^{-1}. To deconvolute the spectral contributions of water and propylene carbonate in the OH stretching region, an intensity normalization and subtraction of the pure propylene carbonate spectrum is performed. For the intensity normalization, a scaling factor, *f*, is calculated for each of the water concentrations studied. This is accomplished by dividing the intensity of the symmetric CH_2 stretching peak (2938 cm^{-1}) in the specific water + PC spectrum by the intensity (at the same peak position) in the pure PC spectrum. The entire pure PC spectrum was then scaled by the resulting ratio

and subtracted from the corresponding water + PC spectrum. This process is carried out mathematically for $\chi_{water} = 0.296$ as follows:

$$f = \left(\frac{I_{\chi = 0.296}\left(2938\ cm^{-1}\right)}{I_{\chi = 0}\left(2938\ cm^{-1}\right)} \right)$$

$$Corrected\ Spectrum = I_{\chi = 0.296} - \left(f \cdot I_{\chi = 0} \right)$$

Figure S2 demonstrates the result of scaling the pure PC spectrum to the intensity of the $\chi_{water} = 0.296$ spectrum as well as the resulting difference ("corrected") spectrum.

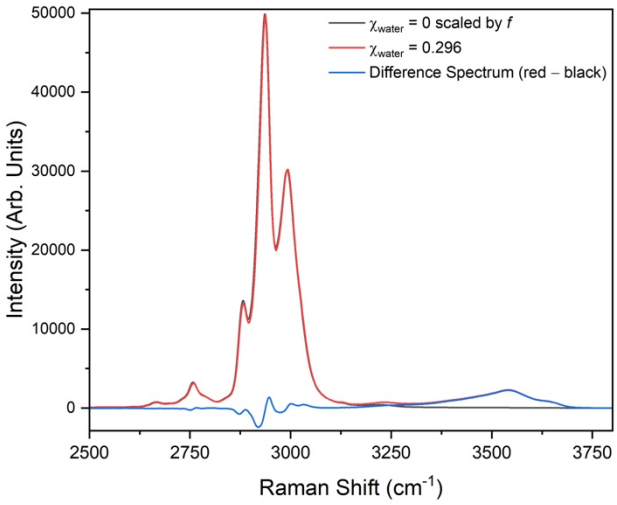

Figure S2. Raman Spectrum of PC + $\chi_{water} = 0.296$ (red), Pure PC ($\chi_{water} = 0$) scaled by the calculated scaling factor, *f* (black), and the resulting spectrum obtained from their subtraction (blue). Subtraction carried out to remove spectral contributions of pure PC from the OH stretching region.

The symmetric CH_2 stretching peak was chosen as the reference point because it is the most intense peak in each of the individual spectra and because the scaling factor obtained using this peak is approximately the average scaling factor obtained when the same process was carried out using the symmetric CH_3 and asymmetric CH_2 stretching peaks as the reference point. After the intensity normalization and subtraction procedure, the spectral contributions from pure PC in the OH stretching region have been removed. The resulting OH stretching bands originating from water are plotted in the main article (Figure 1).

Gaussian Deconvolution

To characterize the hydrogen bond structure of water as a function of its concentration in PC, the OH stretching region was fit using a Gaussian deconvolution procedure in OriginPro 2023. The deconvolution was carried out for 12 of the 25 total spectra, which includes the mole fractions χ_{water} = 0.007, 0.013, 0.024, 0.040, 0.062, 0.091, 0.117, 0.143, 0.190, 0.232, 0.270, and 0.296. The Fit Peaks (Pro) function in OriginLab was used to parametrize and carry out the Gaussian fitting for the OH stretching region between 3073 and 3847 cm^{-1} in each of the 12 spectra. The first step in the parametrization process is defining a baseline for the curve by choosing anchor points along the baseline and an appropriate function to connect the anchor points, effectively fitting the baseline of the data. The wavenumber values 3077, 3096, 3814, and 3843 cm^{-1} were chosen as anchor points for all spectra that were fit. These anchor points were then connected by a linear function. Following this, initial values for the Gaussian peak positions were chosen based on OriginLab's built-in peak-finding function. Once the initialization parameters were set, the Gaussian fitting was carried out until a chi-squared convergence tolerance of 1×10^{-6} was reached. All parameters of the fit were allowed to vary freely apart from the baseline and the peak position of the highest frequency Gaussian. The decision to set the position of the highest frequency Gaussian to a constant value was made after the χ_{water} = 0.143, 0.190, 0.232, 0.270, and 0.296 spectra were initially fit without fixing this parameter. In these fits, the peak position of this Gaussian remained approximately constant, only changing by $\pm$ 0.2 cm^{-1}, which is much smaller that the resolution of the Raman instrument (~4 cm^{-1}). Therefore, the position of this band was set as a fixed parameter for all subsequent fittings. The fit result of the highest water concentration spectrum was used to determine the constant value of the peak position to be 3642.85 cm^{-1}. The lowest frequency band in the OH stretching region did not have a high enough intensity to carry out the fitting (did not converge within 500 iterations) until the concentration χ_{water} = 0.091 was reached, therefore only the seven highest concentration spectra were able to be fit to four total bands.

The lower water concentration spectra are only fit to three bands. In Figure S3, the OH stretching region of the Raman spectra are plotted with the fit result overlaid on the corresponding spectrum. Table S1 contains the converged parameters for all deconvoluted spectra.

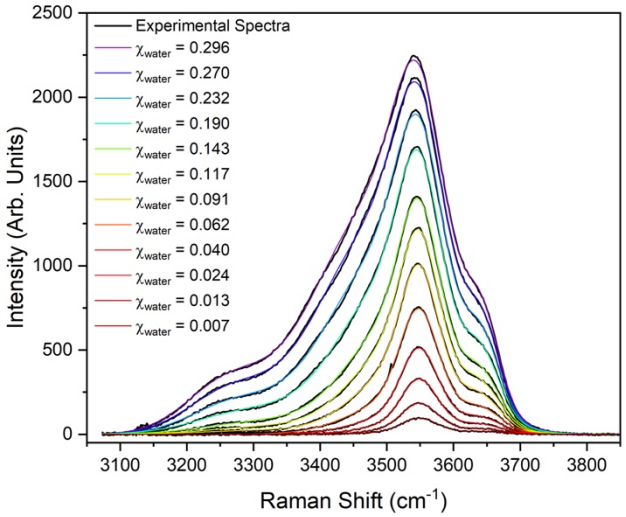

Figure S3. Result of Gaussian fitting to the OH stretching Raman spectra of PC as a function of increasing water concentration. Experimental spectra are plotted in black and calculated (fit) results are in color.

Table S1. Peak center (cm^{-1}), area, intensity (arb. units), and full-width-half-max (FWHM) values obtained from the Gaussian fits of the OH stretching region in the Raman spectra of the PC/water mixtures.

χ_{water}	Center (cm^{-1})	Area	Max. Intensity	FWHM
Peak 1				
0.091	3331.549	5871.516	24.767	222.712
0.117	3329.720	10168.207	45.819	208.482
0.143	3313.961	15339.471	72.718	198.169
0.190	3292.773	25583.312	132.021	182.046
0.232	3274.531	30960.326	184.085	158.000
0.270	3266.546	40439.966	248.489	152.887
0.296	3261.367	46670.106	295.524	148.359
Peak 2				
0.007	3548.494	2272.982	12.437	171.694
0.013	3543.662	5779.104	42.771	126.935
0.024	3540.814	12003.970	77.994	144.588
0.040	3537.119	23089.416	132.327	163.920
0.062	3528.579	40341.990	219.315	172.805
0.091	3526.457	68049.167	397.876	160.673
0.117	3523.554	96854.100	541.741	167.956
0.143	3520.025	128609.003	681.587	177.263
0.190	3509.432	182358.176	899.519	190.451
0.232	3495.311	223349.016	1042.904	201.190
0.270	3485.685	266098.194	1207.844	206.966
0.296	3480.473	299576.228	1326.595	212.147
Peak 3				
0.007	3548.535	5596.160	83.026	63.320
0.013	3549.036	9158.259	141.291	60.893
0.024	3548.803	16421.794	250.442	61.600
0.040	3548.677	25529.054	380.962	62.954
0.062	3548.473	37362.355	534.077	65.720
0.091	3548.915	42541.617	624.894	63.955
0.117	3548.901	48777.053	700.712	65.395
0.143	3548.627	54480.111	758.554	67.471
0.190	3549.084	68665.483	878.296	73.446
0.232	3549.617	89078.920	1024.946	81.647
0.270	3550.014	105598.410	1134.446	87.446
0.296	3550.152	115507.264	1194.283	90.859
Peak 4				
0.007	3642.851	869.162	11.494	71.036
0.013	3642.851	2051.773	25.740	74.885
0.024	3642.851	3372.969	42.166	75.148
0.040	3642.851	4657.074	61.421	71.230
0.062	3642.851	7091.936	98.528	67.620
0.091	3642.851	11228.184	149.198	70.699
0.117	3642.851	13517.129	185.393	68.495
0.143	3642.851	14812.833	214.231	64.957
0.190	3642.851	19628.678	295.670	62.366
0.232	3642.851	25542.695	386.414	62.099
0.270	3642.851	30208.874	458.577	61.886
0.296	3642.851	32249.766	492.302	61.541

Electric field fluctuation decomposition

In the main text, we have used the distribution of electric fields along the OH bond of a water molecular as a map to the Raman lineshape. We have found that these distributions are naturally decomposed into two sub-populations depending on whether the tagged OH bond is donating a hydrogen bond to another water molecule or not. Using the same geometric definition for a hydrogen bond as discussed in the main text, these decomposed distributions are shown in Figure S4 for a range of water concentrations.

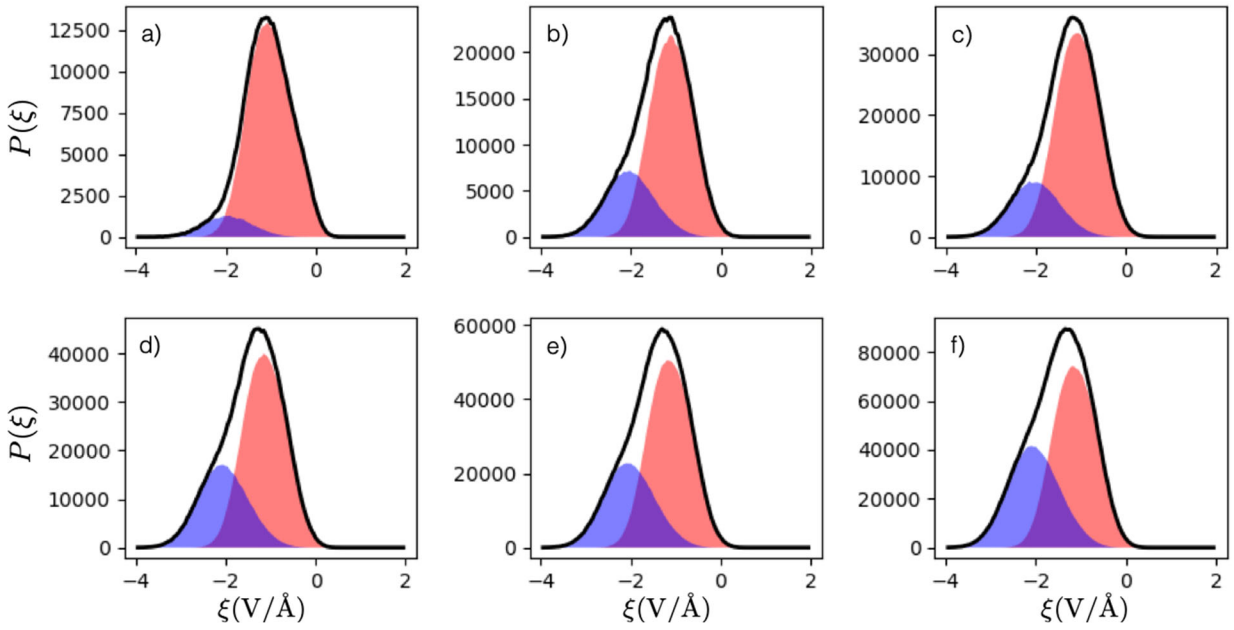

Figure S4. Electric field distributions for water solutions with χ_{water} = a) 0.04, b) 0.08, c) 0.12, d) 0.16, e) 0.19, and f) 0.22 computed from the molecular dynamics simulations discussed in the main text. Shaded regions highlight sub populations for OH oscillators that are donating a hydrogen (blue) or not (red) to another water molecule.